Soft Matter

Accepted Manuscript

ROYAL SOCIETY OF CHEMISTRY

www.rsc.org/softmatter

Journal Name

ARTICLE TYPE

Cite this: DOI: 10.1039/xxxxxxxxxx

Effect of Mechanical-Driven Volumetric Change on Instability Patterns of Bilayered Soft Solids

Shan Tang,*[a‡] Ying Li,[b‡], Yang Yang,[a] and Zaoyang Guo*[c]

Received Date
Accepted Date

DOI: 10.1039/xxxxxxxxxx

www.rsc.org/journalname

If a soft solid is compressible, its volume changes with imposed loading. The extent of the volume change depends on its Poisson's ratio. Here, we study the effect of mechanical-driven volumetric change on buckling and post-buckling behaviors of a hard thin film perfectly bound on a compliant substrate through theoretical analysis and finite element method. The Poisson's ratio of the substrate has been chosen to be in the range of -1 to 0.5, allowing its volume change during deformation. We find that the Poisson's ratio cannot only shift the critical strain for the onset of buckling, but also affect the buckling modes. When the Poisson's ratio of the substrate is close to -1, the surface instabilities of the thin film can be suppressed and delayed to large deformation. The present study demonstrates a new way to control surface instabilities of a bilayered system by changing the Poisson's ratio of the material.

1 Introduction

When a semi-infinite hyperelastic (neo-Hookean) material is under compression, its free surface would become unstable and form sinusoidal waves (wrinkles) upon a critical strain $\varepsilon_{\text{Biot}} = 0.46$[1], according to Biot's linear perturbation analysis with plane strain condition. However, experimental[2–4], theoretical[4,5] and computational[6,7] studies reveal that sharp creases happened on the surface at the critical strain $\varepsilon_{\text{crease}} = 0.35$. The creases, other than wrinkles, are usually observed when a block of an elastomer is bent since $\varepsilon_{\text{crease}} < \varepsilon_{\text{Biot}}$. However, when a stiff thin film attached on a compliant thick substrate is under compression, wrinkles are usually occurred to release the stress (cf. Fig. 1)[8,9]. Wrinkles are surface undulations in the space with infinitesimal strain, while creases are localized self-contacted regions with large strain relative to its initial homogeneous state. Therefore, the cross section of a crease has a very sharp tip, which is distinct from that of a wrinkle. These surface instabilities have been widely applied to control biomolecular pattern and enzymatic activity[10], biofouling[11], interfacial adhesion[12] and cellular behavior[13]. Nevertheless, these instabilities may also lead to failure of materials, such as buckling of microelectromechanical systems[14,15] and composite materials[16,17]. Therefore, it raises a critical question: *How these surface instabilities can be controlled and suppressed?*

As an attempt to answer above question, Cao and Hutchinson have computationally and theoretically studied a bilayer structure with a stiff elastomer film on a polymeric substrate[18]. Their results demonstrate that the critical strain for the onset of wrinkles $\varepsilon_{\text{wrinkle}}$ can be easily tuned via the Young's modulus ratio between the film and substrate E_f/E_s, where E_f and E_s are the moduli for the film and substrate, respectively. For instance, when $E_f/E_s = 20$, $\varepsilon_{\text{wrinkle}} = 0.07$ (refer to Fig. 9 therein)[18]. However, $\varepsilon_{\text{wrinkle}}$ has been dramatically increased to 0.3 for $E_f/E_s = 2$, which is much smaller than $\varepsilon_{\text{Biot}}$ and $\varepsilon_{\text{crease}}$ (refer to Fig. 2 therein)[18]. An unified phase diagram for different surface instabilities of compressed film/substrate systems has been obtained by Wang and Zhao[19], by considering the moduli of the film and substrate, the interfacial adhesion strength, the film thickness and the pre-stretch of the substrate. Although these studies can be used to control the different surface instabilities, the related material failure still cannot be prevented. Very recently, Jin and Suo have shown that the surface creases can be suppressed by the strain-stiffening materials[20]. When the material stiffens deeply at large strains, its surface is initially smooth, then forms creases, and finally becomes smooth as the compressive strain increases. If the material stiffens deeply at small strains, the creases will never occur and be completely suppressed[20]. According to authors' knowledge, the work of Jin and Suo[20] is first study attempted to suppress surface instabilities of materials under large compression, although it relies on the intrinsic mechanical properties of materials, indicating it may not be applicable to many other materials without strain-stiffening.

Growth-induced surface instabilities of layered soft solids attract great interested recently. For a bilayered system with a thin

[a] 174 Shazheng Street, College of Aerospace Engineering, Chongqing University, Chongqing, China. E-mail: stang@cqu.edu.cn.
[b] 2145 Sheridan Road, Department of Mechanical Engineering, Northwestern University, Evanston, USA. E-mail: yingli@u.northwestern.edu.
[c] 37 Xueyuan Road, Institute of Solid Mechanics, Beihang University, Beijing, China. E-mail:z-guo@foxmail.com.
‡ These authors contributed equally to this work.

stiff layer and a thick compliant substrate, the mismatch of the volume expansion between these two layers can lead to compressive stress in a layer, then the free surface of the system is wrinkled to minimize the system energy. For instance, Yin et al.[21,22] simplified the natural fruits and vegetables as a core/shell system with stiff exocarp (shell) and compliant carcocarp (core). The different undulating morphologies found in variety of fruits and vegetables are explained by the volume growth of the inner core. Li et al.[23,24] studied the volumetric growth of mucosal layer in the inner layer of soft tissues such as esophagus, pulmonary airway and many animal lumens. The folding or wrinkling of mucosal layers is explained through the buckling analysis, accounting for the volumetric growth of mucosal layer. The folding or wrinkling pattern may serve as the clinical symptoms of diseases in these organs. Ciarletta et al.[25] further established morphological phase diagrams for pattern selection of tubular tissues due to the growth process by the initiate epithelial differentiation or pathological condition. In these studies, the volumetric change of a layer is described by an extra growth tensor $\mathbf{F}^g$, induced by the molecular diffusion during this process. Then, the total deformation gradient is formulated as $\mathbf{F} = \mathbf{F}^e\mathbf{F}^g$, with $\mathbf{F}^e$ representing the elastic deformation without volumetric change.

Here, we discuss another mechanism of volumetric change on the surface instabilities of a bilayered system under compression. This mechanism origins from the compressibility of polymeric materials. For isotropic materials, the Poisson's ratio ranges from -1 to 0.5. Polymeric materials are usually assumed to be incompressible with Poisson's ratio 0.5. Thus, its volume is conserved under external loadings. However, it is well known that the soft polymeric materials can be compressible, the extent of which depends on the temperature T or its microstructure. For instance, polymers at a temperature T above their glass transition temperature T_g behave like incompressible materials; while they act compressible when $T < T_g$, as elaborated in a recent review by Greaves et al.[26]. The temperature dependent Poisson's ratio for polymeric materials has also been recently conformed by our molecular simulations[27]. Besides, many polymeric materials with negative Poisson's ratio are designed and invented recently[26,28–30]. Polymer gels such as hydrogels can absorb or discharge water molecules, resulting dramatic volumetric changes. Previous study also demonstrated that gels can exhibit negative Poisson's ratio close to -1 near the phase transition[31]. Inspired by these phenomena, we can roughly simplify these materials as hyperelastic soft solids with compressibility. To consider the volumetric changes of these soft solids, the deformation energy of the material is decomposed into the deviatoric and volumetric strain energy parts, which have been discussed in the previous study[32]. Here we should emphasize that all the previous theoretical[1,4,5,8] and computational[6,7,18,19] studies assume that the elastomer is incompressible with Poisson's ratio fixed to be 0.5 for simplifying the surface instability problem.

In this work, we provide a new way to tune the surface instability of a bilayer structure under large compression by changing the compressibility of the substrate. A thin stiff film is coated on a thick compliant substrate for the bilayer structure. Through theoretical analysis, we find that the surface wrinkles can be delayed to a large compressive strain ($\varepsilon_{\text{Biot}}$), if the substrate has a negative Poisson's ratio. Inspired by the theoretical results, we develop a finite element analysis (FEA) model to quantitatively study the surface instability of the thin film/substrate system under compression, with related morphological transition during this process. The FEA results further conform that creases, wrinkles, period doubling and folds (secondary bifurcations after the initial instability, cf. Fig. 1), and other surface instability forms, can be suppressed and delayed to a very large compressive strain $\varepsilon_{\text{Biot}}$. However, these instabilities cannot be delayed when Poisson's ratio of the substrate is positive. Therefore, the Poisson's ratio of the substrate is identified as the key to tune and suppress the surface instabilities of materials during compression. The present study also opens a new way to understand the surface instability behaviors of the thin film/substrate systems, which can be utilized to design stretchable electronics and laminates of packaging materials.

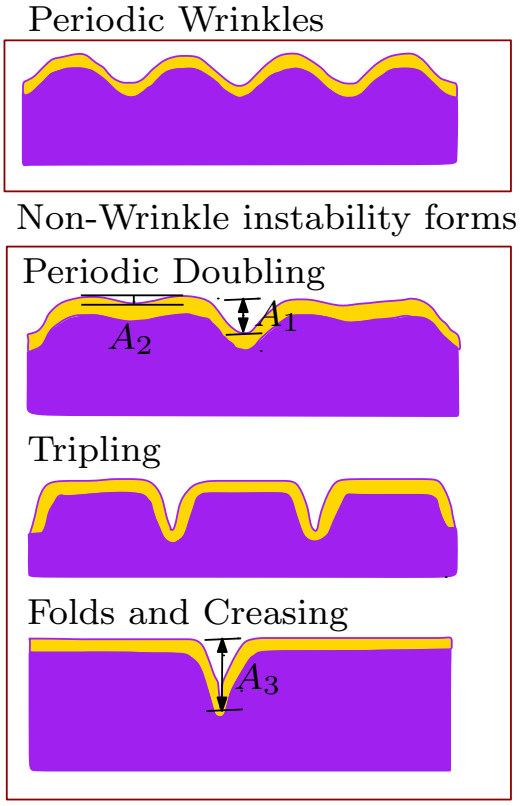

Fig. 1 Typical surface instability patterns for a stiff thin film on a compliant substrate under compression.

2 Model and Methodology

Here we consider a model bilayered system for a thin film coated on a substrate, as shown in Fig. 2. The initial thicknesses of the film and substrate are h and H, respectively. Unless otherwise stated, the thickness ratio h/H is taken to be $1/100$. Both the thin film and substrate are assumed to be homogeneous materials. Note that auxetic materials can be made through introducing the microstructure, such as voids, into polymeric solids or gels. Even with the microstructure, we still assume they behave like

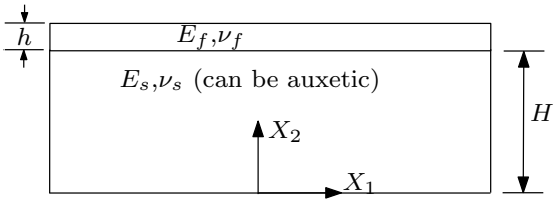

Fig. 2 Schematic of a thin film-substrate system. Both the thin film and substrate are polymeric materials. The Young's modulus and Poisson's ratio are denoted as E and ν, respectively. The subscripts 's' and 'f' represent the substrate and film, respectively. h and H are the thickness of the film and substrate, respectively. Here, we consider that the substrate may has specifically designed microstructure, such as voids. Thus, $-1 < \nu_s < 0.5$. The Poisson's ratio of the film is taken to be 0.499, mimicking the nearly incompressible behavior.

hyperelastic materials. Then, both the thin film and substrate are modeled as compressible neo-Hookean solids with Young's modulus E and Poisson's ratio ν. We adopt the compressible neo-Hookean model with the free energy density:

$$W^H = \frac{\mu}{2}(\bar{I}_1 - 3) + K_m (J-1)^2 \tag{1}$$

where $J = \det \mathbf{F}, \bar{\mathbf{F}} = J^{-1/3}\mathbf{F}$ and $\bar{I}_1 = J^{-2/3} I_1$. I_1 is the first invariant of the left Cauchy-Green tensor $\mathbf{C} = \mathbf{F}^T\mathbf{F}$ and $\mathbf{F}$ is the deformation gradient. μ and K_m are the shear and bulk moduli, respectively. In the small deformation regime, a hyperelastic material will behave like a linear elastic material. Through the above model, the different Poisson's ratio can be realized by adjusting the ratio between μ and K_m, as Young's modulus E and Poisson's ratio ν can be related to μ and K_m through a classical relationship $E = 2\mu(1+\nu)$, $\nu = (3K_m - 2\mu)/[2(3K_m + \mu)]$ for linear elastic materials. The first Piola-Kirchhoff (PK) stress can be obtained by[33]:

$$P_{ij} = \frac{\partial W^H}{\partial F_{ij}}, . \tag{2}$$

for compressible hyperelastic solids. To explore the effect of Poisson's ratio of the substrate on the surface instability, we fix the Poisson's ratio of the thin film to be 0.499 (nearly incompressible), and vary the Poisson's ratio of the substrate from -1 to 0.5.

Baru et al.[34] investigated the nearly incompressible thin film/substrate system under compression. The wrinkles are firstly formed on the surface of the thin film. With the compressive strain further increasing, the surface wrinkles evolve into very complex non-wrinkle patterns such as period doubling, localized folds, creasing and ridges (cf. Fig. 1). These surface instability patterns can be controlled by the modulus ratio between the thin film and substrate[18,35]. In many applications, the thin film is much stiffer than the substrate, with the modulus ratio as high as 10^5. However, when the thin film and substrate are both soft solids, their modules ratio can be moderate, as studied by Cao and Hutchinson[18]. Thus, we mainly focus on the lower stiffness ratio range in present study.

A semi-theoretical algorithm has been proposed for the analysis and prediction of surface instability of multilayered *compressible* polymer plates and sheets under large deformation and plane strain conditions, abandoning the assumption that polymeric materials are incompressible[36]. The proposed algorithm is verified by comparing its predictions with published results in literature for thin films with polymer/metal substrates. This algorithm is adopted to study the instability of the bilayered structure under compression in present study. The analysis is a two-step procedure. We first apply the uniform stretch λ along X_1 direction. Then, the perturbation with all the wavelengths is imposed on the current configurations. Then, the critical strain for the onset of instability with corresponding wavelengths can be obtained. The relevant technique details with mathematical formulations are given in our recent work[36].

To fully understand the other patterns of surface instability, such as period doubling and folds (creasing), during the post-buckling stage, we also carry out the finite element analysis (FEA) by using the commercial finite element software, ABAQUS. We adopt the two-step analysis: (1) linear perturbation (buckling) analysis, followed by (2) post-buckling analysis. The buckling analysis for finite sized domain has been described elsewhere, for example, Refs.[6,27,37,38]. After the buckling modes have been determined from the linear perturbation analysis, an imperfection in the form of the most critical eigenmode (the lowest eigenmode) is introduced into the initial finite element mesh. In this study, the initial mesh is perturbed by the first eigenmode $\hat{v}_1$, scaled with factor $w = 0.05h$. All the finite element meshes have been refined to conform that our simulation results are not sensitive to the mesh size.

3 Results and Discussion

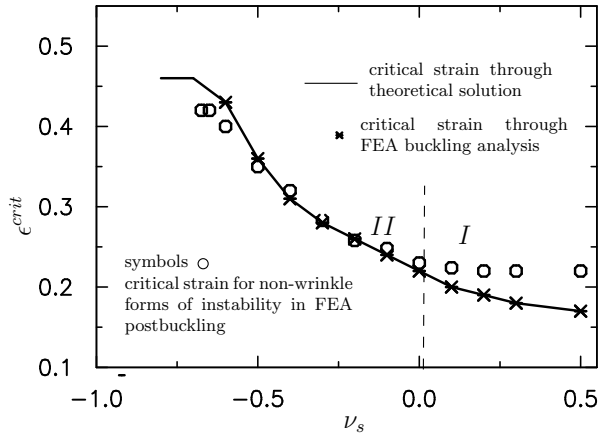

Fig. 3 Critical strain ε^{crit} vs. Poisson's ratio of the substrate ν_s for the fixed modulus ratio $E_f/E_s = 5$.

We first set the modulus ratio $E_f/E_s = 5$. We stress again that the elastic stability analysis is performed by solving the incremental equilibrium equations $\mathrm{Div}\dot{\mathbf{P}} = \mathbf{0}$ with appropriate boundary conditions, where $\dot{\mathbf{P}}$ is the incremental nominal stress. The theoretical solution is obtained by the recently proposed semi-theoretical algorithm[36] to solve the incremental equilibrium equations with appropriate boundary conditions. The theoretically predicted critical strain for the onset of instability is presented in Fig. 3 as a solid line. Here the critical strain is defined as

$\varepsilon^{crit} = 1 - \lambda^{crit}$, which is consistent with the previous study given by Biot[1], Cao and Hutchinson[18]. The critical strain obtained from FEA is also given in Fig. 3, denoted by star symbols, which is consistent with our theoretical prediction. It is clearly shown that the critical strain monotonically decreasing with ν_s increasing from -1 to 0.5, signaling that the substrate with negative Poisson's ratio can dramatically delay the surface instability. When the Poisson's ratio of the substrate is positive, the Poisson's ratio effect on the critical strain is not pronounced; while the critical strain has been dramatically increased from 0.23 to 0.46 when ν_s is reduced from 0.0 to -1. If the Poisson's ratio of the substrate approaches -1, the limitation for the isotropic materials, the critical strain will also reach the limit $\varepsilon_{\text{Biot}} = 0.46$. Although we only show the results for $E_f/E_s = 5$, other cases with different modulus ratios still follow the same trend. All these theoretical results demonstrate that the substrate with a negative Poisson's ratio can help to suppress and delay the surface instability of the attached thin film during compression. However, it is impossible to pass the critical strain $\varepsilon_{\text{Biot}} = 0.46$ without instability. Although we do not have an exact physical explanation on this phenomenon, we suspect that the reduced Poisson's ratio is equivalent to the increased effective modulus $E/(1-\nu^2)$ under plane strain condition. The effective modulus will be extremely large as the Poisson's ratio of the substrate is approaching -1. When the modulus of the substrate is equal or larger than the thin film, the critical strain will be Biot's solution[18].

The effect of substrate Poisson's ratio ν_s can be qualitatively understood in the following way. When $\nu_s > 0$, both the thin film and substrate are compressed along the X_1 direction, while stretched along the X_2 direction due to the Poisson's effect (cf. Fig. 2). Up to certain value of the compressive strain, the surface of the thin film undulates to minimize the free energy of the system[15,39]. However, if the substrate has a negative Poisson's ratio with $\nu_s < 0$, the thin film and substrate will be stretched and compressed along the X_2 direction, respectively. In this way, the undulation of the thin film will be canceled out due to the compression of the substrate and compatibility between the film and substrate (assuming the thin film is perfectly bound to substrate). Therefore, the surface instability can be dramatically suppressed and delayed, when the Poisson's ratio of substrate is close to -1, as observed by our above theoretical and numerical analysis.

The non-wrinkle patterns of surface instability are examined through the post-buckling analysis. In this post-buckling analysis, the initial periodic wrinkles lose their original periodicity through period doubling or folds (creasing) after a secondary critical strain. The secondary critical strain has been recorded as ε^{pw} in our FEA. ε^{pw} is plotted against the Poisson's ratio of the substrate μ_s in Fig. 3 with circle symbols. Comparing with the critical strain at the onset of the periodic wrinkling with ε^{pw}, we can separate the curve of critical strain into two regimes. In the regime I, the critical strain at the onset of instability is lower than ε^{pw}. Thus, the periodic wrinkles occur earlier than the non-wrinkle instabilities, such as period doubling under compression, and gives a way to non-wrinkles at a larger compressive strain. Through the prescription of the cell size and initial imperfection, Auguste et al.[35] compared the energies of periodic wrinkles with period doubling, period quadrupling or tripling for a hard thin film on a compliant substrate with modules ratio $E_f/E_s = 50$. They found that period doubling, period quadrupling or tripling had lower energy than that of period wrinkles. However, in the regime II, the critical strain at onset of instability is nearly the same as ε^{pw}, indicating that the thin film/substrate system is in a bistable state.

Here we should emphasize that the buckling analysis is a different procedure from the post-buckling analysis. In the post-buckling analysis, the imperfection, obtained from the buckling analysis, is introduced in the initial mesh. As discussed in the previous study by Cao and Hutchinson[18], the critical strain obtained from FEM is imperfection sensitive. The critical strain predicted from the post-buckling analysis can be lower than that predicted from the buckling analysis, as shown in Fig. 3.

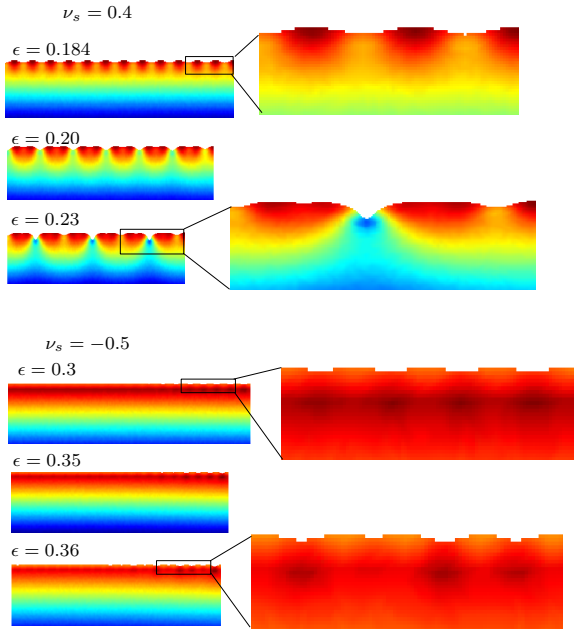

Fig. 4 Evolution of surface morphologies for the thin film/substrate system under compression. The modules ratio E_f/E_s is fixed to be 5. Two different values for the Poisson's ratio of the substrate are considered, 0.4 and -0.5, corresponding to the regimes I and II in Fig. 3, respectively.

Baru et al.[34] studied the secondary critical strain ε^{pw} for a planar bilayered system of hard thin film on soft substrate. ε^{pw} is found to vary with the Poisson's ratio of substrate as $\varepsilon^{pw} = 0.02(1-\nu_s)^2/(1-2\nu_s)^2$. This equation gives a singular solution when the substrate is nearly incompressible with $\nu_s = 0.5$. The trend of ε^{pw} versus ν_s is not consistent with present FEA results. Note that ε^{pw} is increasing with decreasing ν_s is current study. The discrepancy may arise from the simplification of thin film as a shell and the interaction between the film and substrate is simply imposed by a pressure, which is just a linear function of the shell slope in the study by Baru et al.[34]. Although their simplified model can predict the onset of periodic doubling for a stiff film on a complaint substrate, the effect of Poisson's ratio ν_s is not accurately captured. In contrast, our present model does not introduce any simplification on the thin film and interaction between

the film and substrate has been correctly represented, which will enable us to accurately predict the secondary critical strain ε^{pw}. To further clarify this issue, we have theoretical derived the relationship between the critical strain and Poisson's ratio of the substrate in the appendix, though small deformation assumption. The obtained trend follows well with the results given in Fig. 3 (cf. Fig. 9).

We then illustrate the typical instability patterns with different Poisson's ratio of the substrate under a fixed modulus ratio $E_f/E_s = 5$. The evolution of surface morphologies with two different Poisson's ratios $\nu_s = 0.4$ (regime I) and -0.5 (regime II) is given in Fig. 4. For $\nu_s = 0.4$, the periodic wrinkles occur around 0.18, which is consistent with above theoretical and FEA prediction through linear perturbation analysis (cf. Fig. 3). The periodic wrinkles evolve into the doubling-period and folds afterwards. The observed trend is similar to that given by Cao and Hutchinson[18] for a thin stiff film on a thick compliant substrate, while both the thin film and substrate are incompressible. However, when $\nu_s = -0.5$, the surface still maintains flat under large compressive strain. When the compressive strain is close to the critical strain for periodic wrinkles (0.36), the surface wrinkles with very small amplitude have been observed. Note that 0.36 is comparable with the critical strain $\varepsilon_{\text{crease}} = 0.35$ for a homogeneous neo-Hookean solid under compression[4,5]. This is greatly different from what has been observed for the case with $\nu_s = 0.4$.

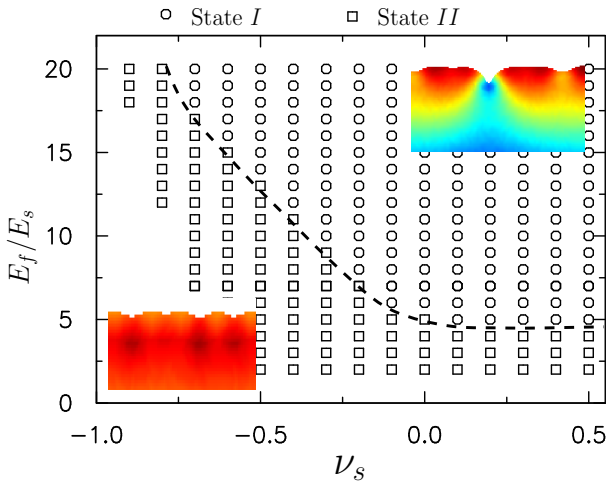

Fig. 5 Phase diagram for a hard thin film on a soft substrate under compression. According to different modulus ratio E_f/E_s and substrate Poisson's ratio ν_s, two different regimes have been identified (cf. Fig. 3), which is separated by the dashed line.

According to the above simulation results, we notice that two dimensionless parameters: modulus ratio E_f/E_s and the substrate Poisson's ratio ν_s primarily affect the instability patterns. To explore how the instability pattern varies with these two parameters E_f/E_s and ν_s, a phase diagram is given in Fig. 5. Two different regimes (regimes I and II shown in Fig. 3) have been identified and marked as the circles and squares, respectively. The phase boundary between these two regimes is denoted by a dashed line. When the modulus ratio E_f/E_s is fixed, with the increasing ν_s, the periodic doublings and folds are more pronounced after initial periodic wrinkles. When E_f/E_s is less than 5, it is always observed that the instability pattern within regime II. In consistent with Baru et al.[34] and Auguste et al.[35], the modulus ratio in their theoretical analysis and experiments is larger than 5 to observe the evident periodic doublings and folds.

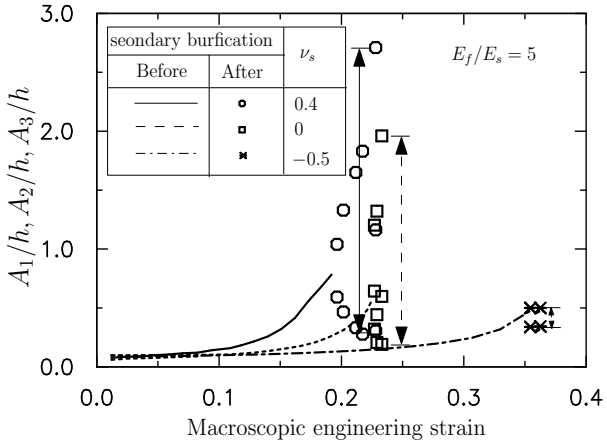

Fig. 6 Amplitude of surface instabilities (A1, A2, A3) as a function of the imposed strain with three different Poisson's ratios of the substrate. A1, A2 and A3 are defined in Fig. 1.

In the above section, we have examined the instability patterns and the critical strain for the onset and evolution of the periodic wrinkles and non-wrinkles caused by the volumetric change of the substrate. We then explore how the volumetric change can affect the amplitude of surface wrinkles. The amplitude of these wrinkles (A1, A2 and A3, cf. Fig. 1) is given in Fig. 6 with fixed modules ratio $E_f/E_s = 5$ and three different Poisson's ratios $\nu_s = 0.4$, 0, -0.5. According to the previous study by Baru et al.[34], when the imposed macroscopic strain is larger than the secondary critical strain ε^{pw}, periodic doubling always occurs. Therefore, the amplitude of surface wrinkles bifurcates into two different values. One represents large wrinkles and the other denotes superimposed small wrinkles (cf. Figs. 1 and 4). With imposed compressive strain further increases, some of large wrinkles evolve into folds. The amplitude of folds is even larger than these wrinkles, which is several times of the film thickness h. These observations are correct for the case with $\nu_s = 0.4$ and 0, as shown in Fig. 6. When $\nu_s = -0.5$, the small surface wrinkles cannot evolve into the folds with large amplitude. Thus, the amplitude of the surface instability is comparable with the film thickness h.

Recent experimental and computational studies suggest that wrinkling patterns may vary strongly with the surface curvature[40]. To explore the surface curvature effect, we further investigate the effect of Poisson's ratio on the instability pattern of the bilayered structure with another surface curvature. A model of the polymeric cylinder with a core/shell structure under compression is given in Fig. 7. The length of the cylinder in the initial and current configurations are L_0 and L, respectively. The thickness of the shell layer is δ. The inner and outer radii are R_i and R_o, respectively. We fix $L_0/R_o = 3$. FEA has been carried out to

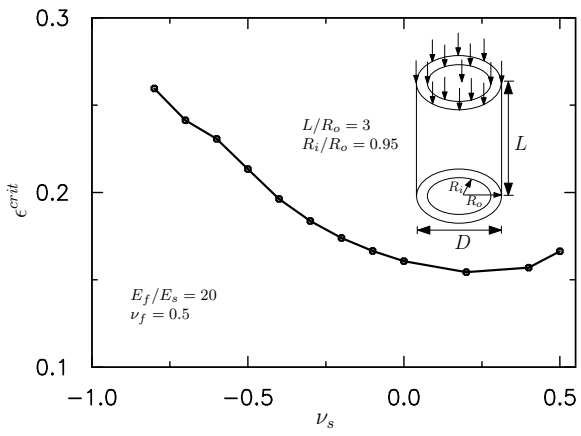

Fig. 7 Critical strain ε^{crit} vs. the Poisson's ratio of inner core ν_s for a cylindrical core/shell system under compression. The modulus ratio between the shell and core layers is fixed to be 20.

explore the buckling and post-buckling behaviors of the cylinder under compression. The Poisson's ratio for the shell is set to be 0.499 (nearly incompressible) and the value for the core layer is varied in FEA. The modulus ratio between the shell and core layers is fixed to be 20. The top of the cylinder is under compression, while the bottom is fully fixed in the simulation.

The obtained critical strain at the onset of surface wrinkles is given in Fig. 7 as a solid line. The critical strain is also defined as $\varepsilon^{crit} = 1 - \lambda^{crit}$. Again, the critical strain is monotonically decreasing with the Poisson's ratio of the core layer increasing from -1 to 0.5, similar to the thin film/substrate system given in Fig. 3.

The buckling modes with four different Poisson's ratios of the inner core, eigenmode I to eigenmode III, are given in Fig. 9a. For Poisson's ratio of the inner core as 0.5 and -0.5, the cylinder exhibits instability patterns with periodic wrinkles along its axial direction. Bigoni and Gei[41] theoretically studied the instability of *incompressible* core/shell systems. The obtained instability pattern is consistent with present study on the short cylinder with $L_0/R_o = 3$. However, for the Poisson's ratio -0.8, we observe that tilting buckling dominates (cf. Fig. 9a). More interestingly, the eigenmode III exhibits wrinkling patterns along the circumferential direction, instead of the axial direction. When the Poisson's ratio is further reduced to -0.9, we cannot obtain the buckling modes under compression through the linear perturbation analysis. In summary, the Poisson's ratio of the core can be used to tune the buckling models for the bilayered system with curved surface.

After the buckling modes have been determined through the linear perturbation analysis, an imperfection in the form of the most critical eigenmode (the lowest eigenmode) is introduced to the mesh for post-buckling analysis. The initial mesh is perturbed by the first eigenmode $\hat{v}_1$ with scale factor $w = 0.05\delta$ (for the inner core with Poisson's ratio -0.9, we impose the buckling modes from that with Poisson's ratio -0.8). The deformation morphologies at the moment when the buckling takes place in the post-buckling analysis are demonstrated in Fig. 9b, with four different Poisson's ratios. Consistent with previous buckling analysis,

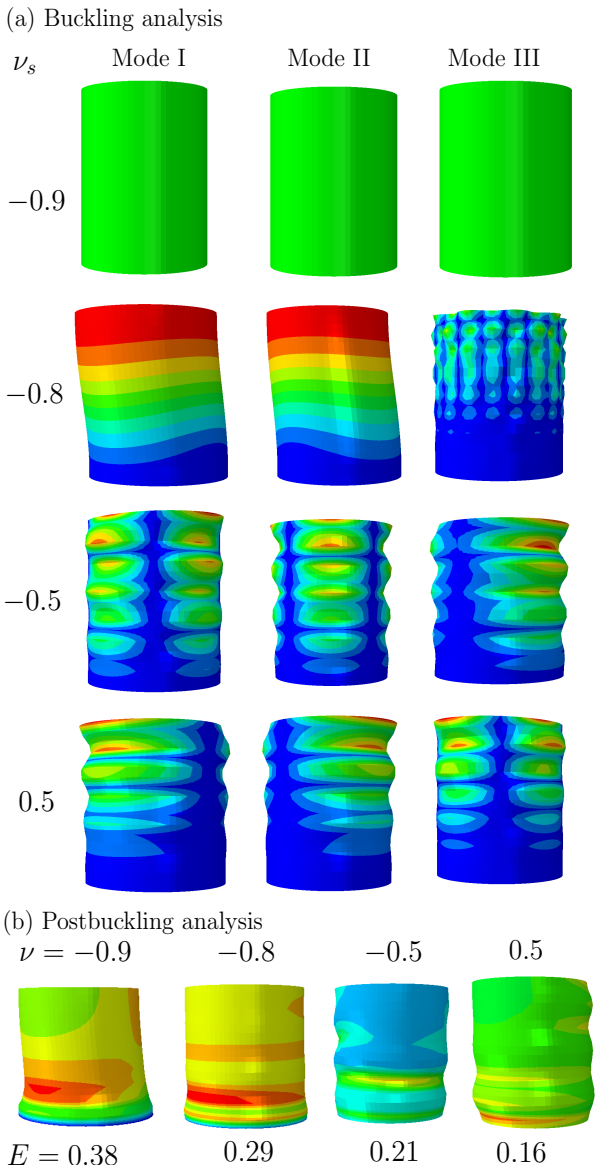

Fig. 8 (a) Buckling modes I - III for four different Poisson's ratios of the inner core; (b) instability patterns at the moment where buckling takes place from the FEA in the post-buckling analysis.

the critical strain at onset of buckling increases with decreasing Poisson's ratio of the inner core. Periodic wrinkles along the axial direction give way to the tilting buckling patterns, when the Poisson's ratio of inner core is reduced. In comparison with the planar bilayered system, we do not observe the secondary buckling during the post-buckling analysis, even for incompressible inner core. This may suggest the curved surface can prevent the secondary buckling. A thorough study will be performed to illustrate the surface curvature effect, as we only consider one ratio of length over diameter in this study.

4 Concluding Remarks

Through the theoretical analysis and finite element simulation, we explore the effect of volumetric change on surface instability of a bilayered system under compression. The thin film and substrate are taken to be incompressible and compressible, re-

spectively, to reveal the effect of substrate Poisson's ratio. We find that the surface instability of the thin film/substrate system can be suppressed and delayed, when the substrate Poisson's ratio is negative. The post-buckling behaviors of the bilayered system is also greatly affected by the Poisson's ratio of the substrate. Thus, the mechanical-driven volumetric change of the substrate can be used to tune the surface instability patterns of the bilayered system under compression.

In previous studies, the polymeric substrate has been used to enhance the stretchability of metallic and semiconducting thin films[42–44]. For example, the copper thin films deposited on Kapton substrates can be stretched beyond 0.5[42], since the strain localization in the thin film can be retarded by the substrate. In another way, by attaching the silver thin films on the elastomer substrates with sinusoidal ('wavy') surface features, they can be easily stretched up to 0.46[43]. All these studies can be used for the design of stretchable electronics[45]. In contrast to these studies, we provide a new way to enhance the compressibility of elastomer thin films by suppressing and delaying their surface instabilities under compression. With the help of an auxetic substrate, which has a very small negative Poisson's ratio (-1), the elastomer thin films could be compressed up to 0.46 without occurring evident surface instabilities. It opens a way for the design of stretchable electronics, since compression is as important as tension[46].

Appendix: Linear Elastic Theory on Surface Instability of a Bilayered Structure with Poisson's Ratio Effect

In the main text, the theoretical analysis was formulated according to the strict finite deformation theory[36]. It is very difficult to obtain a close mathematic expression even when both the film and substrate are incompressible, as discussed by Cao and Hutchinson[18]. To provide a detailed insight into the effect of Poisson's ratio on instability of a bilayered structure, we drive a mathematic expression for the critical strain as a function of the material and geometric parameters, according to the small deformation assumption.

When an uniform compressive deformation e_0 is imposed on the bilayered structure without buckling, the deformation energy of the thin film/substrate with length L takes the following form under plane strain deformation:

$$W_{uni}=\frac{1}{2}\frac{E_f e_0^2}{\left(1-v_f^2\right)}Lh+\frac{1}{2}\frac{E_s e_0^2}{\left(1-v_s^2\right)}LH$$

where h and H are the thickness of thin film and substrate, respectively. Note that we use the subscript f and s denoting the thin film and substrate, respectively.

Upon a critical compressive strain, the uniform deformation gives a way to the wrinkling. Let's assume that perturbation deformation fields are given in the following:

$$\begin{aligned} x &= X \\ y &= Y+F(Y)\,g(X) \end{aligned}$$

where (x,y) and (X,Y) are the coordinates in the current and original configurations, respectively. F is a function of Y and g is a function of X. Under the small deformation assumption, the strains are given by

$$\varepsilon_{xx}=0 \qquad \varepsilon_{yy}=F^{'}g \qquad \varepsilon_{xy}=\frac{1}{2}Fg^{'} \tag{3}$$

where the $'$ represents the derivatives. Then, the stored elastic energy for the perturbation deformation fields is:

$$\begin{aligned} W_{buck} &= \int\frac{1}{2}\sigma_{ij}\varepsilon_{ij}dV \\ &= \int\frac{1}{2}\frac{E_s(1-v_s)\left(F^{'}g\right)^2}{(1+v_s)(1-2v_s)}+G_s\left(Fg^{'}\right)^2dV_s+ \\ &\quad \int\frac{1}{2}\frac{E_f\left(1-v_f\right)\left(F^{'}g\right)^2}{\left(1+v_f\right)\left(1-2v_f\right)}+G_f\left(Fg^{'}\right)^2dV_f \end{aligned} \tag{4}$$

where V_s and V_f represent the domains of substrate and thin film, respectively. The perturbation deformation results in

$$e_0=-\frac{\frac{1}{2}\int g^{'2}dx}{L}.$$

If we further assume that F and g take

$$\begin{aligned} F(y) &= \begin{cases} A_0-\frac{A_0-A^I}{h^2}(H+h-y)^2 & \text{in the thin film} \\ A^I\exp\left[-\beta\left(1-\frac{y}{H}\right)\right] & \text{in the substrate} \end{cases} \\ g &= \sin\left(\frac{2n\pi x}{L}\right) \end{aligned}$$

where A_0 and A^I are amplitudes of wrinkles on the top of free surface and interface between the thin film and substrate, respectively. β is a introduced coefficient. The assumed F and g satisfy the boundary conditions (traction free on the top surface; displacement and traction continuity at the interface), as on the top surface $y=H+h$

$$F^{'}=0$$

and at the interface $y=H$

$$\begin{aligned} F\big|_{y\to H^+} &= F\big|_{y\to H^-} \\ \frac{E_t(1-v_t)F^{'}\big|_{y\to H^+}g}{(1+v_t)(1-2v_t)} &= \frac{E_b(1-v_b)F^{'}\big|_{y\to H^-}g}{(1+v_b)(1-2v_b)} \end{aligned} \tag{5}$$

With the assumed deformation fields, the stored elastic energy (Eq. 4) becomes:

$$\begin{aligned} W_{buck} &= \frac{1}{2}\frac{E_s(1-v_s)}{(1+v_s)(1-2v_s)}\frac{A_0^2\gamma^2\beta^2}{H^2}\frac{L}{2}\frac{H(1-\exp(-2\beta))}{2\beta} \\ &\quad +G_sA_0^2\gamma^2\frac{2\pi^2n^2}{L}\frac{H(1-\exp(-2\beta))}{2\beta}+ \\ &\quad \frac{E_f\left(1-v_f\right)}{\left(1+v_f\right)\left(1-2v_f\right)}\frac{(1-\gamma)^2A_0^2L}{3h}+G_fA_0^2\frac{2\pi^2n^2}{L}\frac{3\gamma^2+4\gamma+8}{15}h \end{aligned}$$

where $\gamma = A^I/A_0$ is determined from the Eq. (5)

$$\gamma = \frac{1}{1+\beta\frac{h}{H}\frac{E_s(1-v_s)(1+v_f)(1-2v_s)}{2E_f(1-v_f)(1+v_s)(1-2v_s)}}$$

When the wrinkling takes place,

$$W_{uni} - W_{buck} = 0$$

Then

$$A_0^2 = \frac{\left(\frac{1}{2}\frac{E_s(1-v_s)}{(1+v_s)(1-2v_s)}\frac{\gamma^2\beta^2}{H^2}\frac{L}{2}\frac{H(1-\exp(-2\beta))}{2\beta} + G_s\gamma^2\frac{2\pi^2n^2}{L}\frac{H(1-\exp(-2\beta))}{2\beta}\right) + \frac{E_f(1-v_f)}{(1+v_f)(1-2v_f)}\frac{(1-\gamma)^2L}{3h} + G_f\frac{2\pi^2n^2}{L}\frac{3\gamma^2+4\gamma+8}{15}h}{\frac{1}{2}\frac{E_f\pi^4n^4}{(1-v_f^2)L^3}h + \frac{1}{2}\frac{E_s\pi^4n^4}{(1-v_s^2)L^3}H}$$

Finally, the critical strain for the onset of wrinkle can be obtained:

$$\varepsilon^{crit} = -\frac{A_0^2\pi^2n^2}{L^2} \quad (6)$$

$$= -\frac{\frac{1}{4\pi^2}\frac{(1-v_s)\gamma^2\beta^2}{(1+v_s)(1-2v_s)}\frac{L}{H}\frac{(1-\exp(-2\beta))}{2\beta}\frac{1}{n^2} + \frac{\gamma^2}{(1+v_s)}\frac{H}{L}\frac{(1-\exp(-2\beta))}{2\beta} + \frac{1}{3\pi^2}(1-\gamma)^2\frac{E_f}{E_s}\frac{(1-v_f)}{(1+v_f)(1-2v_f)}\frac{L}{h}\frac{1}{n^2} + \frac{E_f}{E_s}\frac{1}{(1+v_f)}\frac{h}{L}\frac{3\gamma^2+4\gamma+8}{15}}{\frac{1}{2}\frac{E_f}{E_s}\frac{1}{(1-v_f^2)}\frac{h}{L} + \frac{1}{2}\frac{1}{(1-v_s^2)}\frac{H}{L}}$$

By using the same material and geometric parameters as adopted in Fig. 3, the predicted critical strain vs. Poisson's ratio of the substrate with several different β and n values are given in Fig. 9. The critical strain is increasing with the Poisson's ratio of the substrate decreasing, which follows the same trend shown in Fig. 3. According to Eq. 6, the term $1/(1+v_s)$ in the numerator increases much faster than the term $1/(1-v_s^2)$ in the denominator when v_s is decreasing. Note we did not try to tune the parameters β and n to match the results from finite element analysis, since we only want to show the trend. When the substrate is nearly incompressible ($v_s \approx 0.5$), the predicted critical strain approaches infinity, similar to the results given by Baru et al.[34]. This is not correct as the assumed deformation fields do not satisfy the incompressible condition in the small deformation regime $\varepsilon_{xx} + \varepsilon_{yy} \neq 0$. The theoretical analysis obtained from strict finite deformation theory in the main text gives accurate predictions, comparing with the finite element results. Although the simplified linear elastic theory needs to be refined to consider the nonlinearity during finite deformation, it gives a direct physical insight into the problem.

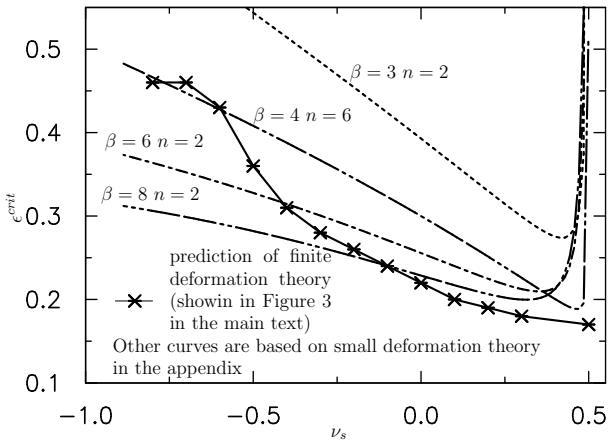

Fig. 9 Critical strain vs. Poisson's ratio of the substrate according to the small deformation theory in comparison with the results shown in Fig. 3 given by the strict finite deformation theory.

Acknowledgment

S.T. thanks NSF of Chongqing (Project No. 0211002431039) and NSF of China (Project No. 11472065) for the support of this study. Y.L. warmly thanks the financial support provided by Ryan Fellowship and Royal E. Cabell Terminal Year Fellowship at Northwestern University. Discussion with Prof. Yueguang Wei (Institute of Mechanics, CAS) is greatly acknowledged.

References

1 M. Biot, *Appl. Sci. Res.*, 1963, **12**, 168–182.
2 A. Gent and I. Cho, *Rubber Chem. Technol.*, 1999, **72**, 253–262.
3 A. Ghatak and A. L. Das, *Phys. Rev. Lett.*, 2007, **99**, 076101.
4 W. Hong, X. Zhao and Z. Suo, *Appl. Phys. Lett.*, 2009, **95**, 111901.
5 E. Hohlfeld and L. Mahadevan, *Phys. Rev. Lett.*, 2011, **106**, 105702.
6 Y. Cao and J. W. Hutchinson, *Proc. R. Soc. London, Ser. A*, 2011, rspa20110384.
7 W. Wong, T. Guo, Y. Zhang and L. Cheng, *Soft Matter*, 2010, **6**, 5743–5750.
8 H. Mei, R. Huang, J. Y. Chung, C. M. Stafford and H.-H. Yu, *Appl. Phys. Lett.*, 2007, **90**, 151902.
9 J.-Y. Sun, S. Xia, M.-W. Moon, K. H. Oh and K.-S. Kim, *Proc. R. Soc. London, Ser. A*, 2012, **468**, 932–953.
10 J. Kim, J. Yoon and R. C. Hayward, *Nat. Mater.*, 2010, **9**, 159–164.
11 P. Shivapooja, Q. Wang, B. Orihuela, D. Rittschof, G. P. López and X. Zhao, *Adv. Mater.*, 2013, **25**, 1430–1434.
12 E. P. Chan, J. M. Karp and R. S. Langer, *J. Polym. Sci., Part B: Polym. Phys.*, 2011, **49**, 40–44.
13 K. Saha, J. Kim, E. Irwin, J. Yoon, F. Momin, V. Trujillo, D. V. Schaffer, K. E. Healy and R. C. Hayward, *Biophys. J.*, 2010, **99**, L94–L96.
14 S. Krylov, B. R. Ilic, D. Schreiber, S. Seretensky and H. Craighead, *J. Micromech. Microeng.*, 2008, **18**, 055026.
15 Y. Li, X.-S. Wang and X.-K. Meng, *Appl. Phys. Lett.*, 2008, **92**, 131902.
16 V. V. Bolotin, *Composites Part B*, 1996, **27**, 129–145.
17 Y. Hu, A. Hiltner and E. Baer, *Polym. Compos.*, 2004, **25**, 653–661.
18 Y. Cao and J. W. Hutchinson, *J. Appl. Mech.*, 2012, **79**, 031019.
19 Q. Wang and X. Zhao, *J. Appl. Mech.*, 2014, **81**, 051004.
20 L. Jin and Z. Suo, *J. Mech. Phys. Solids*, 2015, **74**, 68–79.

21 J. Yin, Z. Cao, C. Li, I. Sheinman and X. Chen, *Proc. Natl. Acad. Sci. U.S.A.*, 2008, **105**, 19132–19135.

22 J. Yin, X. Chen and I. Sheinman, *J. Mech. Phys. Solids*, 2009, **57**, 1470–1484.

23 B. Li, Y.-P. Cao, X.-Q. Feng and H. Gao, *Soft Matter*, 2012, **8**, 5728–5745.

24 B. Li, F. Jia, Y.-P. Cao, X.-Q. Feng and H. Gao, *Phys. Rev. Lett.*, 2011, **106**, 234301.

25 P. Ciarletta, V. Balbi and E. Kuhl, *Phys. Rev. Lett.*, 2014, **113**, 248101.

26 G. N. Greaves, A. Greer, R. Lakes and T. Rouxel, *Nat. Mater.*, 2011, **10**, 823–837.

27 S. Tang, Y. Li, W. K. Liu and X. X. Huang, *Macromolecules*, 2014, **47**, 6503–6514.

28 G. W. Milton, *J. Mech. Phys. Solids*, 1992, **40**, 1105–1137.

29 J. Grima, A. Alderson and K. Evans, *Phys. Status Solidi B*, 2005, **242**, 561–575.

30 S. Babaee, J. Shim, J. C. Weaver, E. R. Chen, N. Patel and K. Bertoldi, *Adv. Mater.*, 2013, **25**, 5044–5049.

31 S. Hirotsu, *J. Chem. Phys.*, 1991, **94**, 3949–3957.

32 E. Arruda and M. Boyce, *J. Mech. Phys. Solids*, 1993, **41**, 389–412.

33 T. Belytschko, B. Moran and W. K. Liu, *Nonlinear finite element analysis for continua and structures*, Wiley, 1999, vol. 1.

34 F. Baru, H. Vandeparre, A. Sabbah, C. Pouland, A. Boudaoud and P. Damman, *Nat. Phys.*, 2011, **7**, 56.

35 A. Auguste, L. Jin, Z. Suo and R. Hayward, *Soft Matter*, 2014, **10**, 6520.

36 S. Tang, Y. Yang, X. H. Peng, W. K. Liu, X. X. Huang and K. Elkhodary, *Comput. Mech.*, 2015, **56**, 63–75.

37 S. Tang, M. S. Greene, X. H. Peng, W. K. Liu and Z. Y. Guo, *Europhys. Lett.*, 2014, **106**, 36002.

38 S. Tang, S. M. Greene, W. K. Liu, X. H. Peng and Z. Guo, *J. Appl. Mech.*, 2015.

39 Y. Li, X.-S. Wang and Q. Fan, *Int. J. Eng. Sci.*, 2008, **46**, 1325–1333.

40 N. Stoop, R. Lagrange, T. Denis, P. Reis and J. Dunkel, *Nat. Mater.*, 2015, **1**, 1–5.

41 D. Bigoni and M. Gei, *Int. J. Solids Struct.*, 2001, **38**, 5117–5148.

42 N. Lu, X. Wang, Z. Suo and J. Vlassak, *Appl. Phys. Lett.*, 2007, **91**, 221909.

43 J. Xiao, A. Carlson, Z. Liu, Y. Huang, H. Jiang and J. Rogers, *Appl. Phys. Lett.*, 2008, **93**, 013109.

44 D.-H. Kim, J.-H. Ahn, W. M. Choi, H.-S. Kim, T.-H. Kim, J. Song, Y. Y. Huang, Z. Liu, C. Lu and J. A. Rogers, *Science*, 2008, **320**, 507–511.

45 J. A. Rogers, T. Someya and Y. Huang, *Science*, 2010, **327**, 1603–1607.

46 F. Xu, W. Lu and Y. Zhu, *ACS Nano*, 2010, **5**, 672–678.